Applied Catalysis B: Environmental 337 (2023) 122991

Contents lists available at ScienceDirect

Applied Catalysis B: Environmental

journal homepage: www.elsevier.com/locate/apcatb

# H-ZSM-5 Catalysts for the catalytic upcycling of polypropylene glycol

Kanan Shikhaliyev [a], Thossaporn Onsree [a], Andrew H. Jaeschke [a], Seyed Majid Ghoreishian [a], Kaveh Shariati [a], Abraham Martinez [b], Alexander Katz [b], Sonjong Hwang [c], Anne Gaffney [d], Jagoda M. Urban-Klaehn [d], Jochen Lauterbach [a,*]

[a] Department of Chemical Engineering, University of South Carolina, Columbia, SC, USA
[b] Department of Chemical and Biomolecular Engineering, UC Berkeley, Berkeley, USA
[c] Division of Chemistry and Chemical Engineering, California Institute of Technology, Pasadena, CA, USA
[d] Energy & Environment S&T Department, Idaho National Lab, Idaho Falls, USA

ARTICLE INFO

*Keywords:*
Catalytic cracking
Polypropylene glycol
Plastic upcycling
Zeolite
Oxygenated polymers
Positron lifetime

ABSTRACT

Without effective management, the steady increase of waste plastics threatens environmental well-being and ecological balance. Plastic up/recycling is a promising solution but has many challenges. In this work, catalytic cracking of polypropylene glycol (PPG) was investigated at varying reaction temperatures of 350–550 °C under nitrogen and steam, using H-ZSM-5 zeolites with different silica-to-alumina ($SiO_2/Al_2O_3$) ratios of 23:1 and 50:1. The catalysts were assessed through physisorption, chemisorption, solid-state magic-angle spinning nuclear magnetic resonance spectrometry, thermogravimetry, electron microscopy, and positron annihilation lifetime spectroscopy. Extra framework aluminum and Lewis-to-Bronsted acid site ratios were found to play a significant role in the selectivity towards propionaldehyde, where values ~ 80 % could be reached. In addition, a possible pathway for the PPG cracking reaction was proposed, which may lead to a better understanding of PPG and waste plastic decomposition via zeolite-based catalysts.

## 1. Introduction

Interest in new approaches for plastics upcycling is growing as an emerging alternative for plastic-waste management [1]. The core idea is converting post-customer plastics into new chemicals, materials, and fuels with high-quality/value. The chemical upcycling reactions of waste plastics are generally conducted in the presence of a hydrothermally stable catalyst allowing for the selective formation of desired higher-value products [2]. Current techniques in plastics recycling realm have significant limitations. For instance, they cannot be scaled at the current rate of waste generated, and approximately 78 % (4.9 billion tons) of waste plastics have been disposed of in landfills or, worse, persist continually elsewhere in the environment [3,4]. Large-scale plastic production has existed since the 1950 s, yet end-of-life plastic treatment methods are still quite limited [4,5]. In 2015, for example, a mere 8.8 % of commercially produced plastics were recycled in the United States [5]; it is expected that the amount of waste recycled and the amount of waste produced globally will continue to drastically increase over the next few decades [4]. With little to no recycling methods for over half of the plastic produced in the United States, there is an emerging opportunity to use solid catalysts to facilitate plastic upcycling through conventional catalytic cracking techniques. One type of plastic in need of recycling is oxygenated waste polymers, which can be found in abundance in insulation, coatings, foams, mattresses, footwear, adhesives, etc. Although the oxygen incorporated into such molecules, in principle, holds promise for more highly selective cracking to chemical products compared with hydrocarbon-based plastics (such as polyethylene and polypropylene) and up/recycling processes for oxygenated polymers remain rare and challenging [6,7].

Catalytic cracking is a conversion process where complex, longer chain molecules are broken down into smaller molecules, and more valuable products in the presence of a catalyst are formed. This process has been used to crack hydrocarbons using zeolite catalysts since the 1960s [8,9], through fluidized catalytic cracking (FCC) units operating at elevated temperatures [9–16]. Zeolites are utilized throughout oil and gas refining (dewaxing, reforming isomerization, and alkylation) [1], while also holding promise in emerging applications, including biomass conversion, methane conversion, and waste plastic upcycling via pyrolysis and catalytic cracking [17–20]. In the case of the latter, much of the research is geared toward thermoplastics, emphasizing

* Corresponding author.
*E-mail address:* lauteraj@cec.sc.edu (J. Lauterbach).

https://doi.org/10.1016/j.apcatb.2023.122991
Received 6 April 2023; Received in revised form 8 June 2023; Accepted 11 June 2023
Available online 12 June 2023

gasoline-range hydrocarbon production as well as other valuable liquid and gas products [13–16,20], while minimizing the production of char [13,15–17]. In the case of plastics, reaction conditions are similar to industrial FCC units (400–600 °C) as these temperatures enable zeolitic activation and cleavage of C—C and C—O bonds [15,16,21]. Many of these processes group the products into categories, such as paraffin, olefins, aromatics, etc., emphasizing selectivity improvement of a specific chemical or group of chemicals [15,16,21]. Therefore, zeolites play a significant role in research geared toward waste plastics upcycling and recycling [12–16,20].

Oxygenated polymer decomposition produces many different types of products, making it difficult to understand the chemical pathways and mechanisms at play. One of the simplest oxygenated polymers is polypropylene glycol (PPG), which is produced from propylene oxide – a chemical that is second in propylene utilization only to polypropylene. A promising selective recycling path for PPG was demonstrated by Gaffney *et al.* [22], who reported that the catalytic treatment of PPG produced valuable chemical products that could be achieved in a fluidized bed reactor with zeolite catalysts, such as Zeolite Socony Mobil-5 (ZSM-5). They also indicated a significant potential for the deconstruction of waste polymers into propionaldehyde. However, the mechanism/pathway of the PPG decomposition and relationships between H-ZSM-5 zeolite properties and selectivity of resulting products have not been investigated in detail.

In this work, catalytic cracking of PPG using H-ZSM-5 zeolites was assessed in a fixed bed reactor by varying reaction temperatures (350–550 °C) under nitrogen and changing amounts of steam in the existence of H-ZSM-5 zeolites with two different $SiO_2/Al_2O_3$ ratios of 23:1 and 50:1. To understand relationships between catalyst properties and product selectivity, the H-ZSM-5 catalysts were examined by employing physisorption, chemisorption, solid-state magic-angle spinning (MAS) nuclear magnetic resonance (NMR) spectroscopy, thermogravimetry (TG), scanning electron microscopy (SEM), X-ray diffraction (XRD), and Positron Annihilation Lifetime (PAL) spectroscopy analysis. Based on these data, we proposed a possible pathway for the thermal and catalytic decomposition of PPG over H-ZSM-5 catalysts.

## 2. Material and methods

### 2.1. Materials and chemicals

PPG with $M_n \sim 425$ was purchased from Sigma-Aldrich and was used as a reactant. Even if PPG $M_n \sim 425$ can still be considered a shorter oligomer, it serves as a model polymer for oxygenated waste plastics for catalytic cracking experiments. $NH_4$-ZSM-5 was purchased from Alpha Aesar and evaluated with two different $SiO_2/Al_2O_3$ ratios (23:1 and 50:1). Both catalysts were calcined at 550 °C for four hours to convert the ammonium form of the zeolite to the hydrogen form (H-ZSM-5).

### 2.2. Experimental setup

Fig. 1**a** shows the home-built reactor system, which consists of a mixer, reactor, and condenser. A high-performance liquid chromatography (HPLC) pump controlled the flow rates of water into the mixer for steam production, while control of the inert nitrogen gas was done by a mass flow controller. The mixer was wrapped with quartz wool high-temperature heating tape, insulation, and aluminum foil for a more uniform heating distribution. It was operated at temperatures over 120 °C, which was assumed to produce a well-mixed carrier gas feed of steam and nitrogen. The gas then flowed to the reactor through a stainless-steel tube and heated at the same temperature as the mixer. Along the way to the reactor, a pressure gauge was installed to monitor the system pressure. The reactor was made of a 316 stainless-steel tube with 12.7 mm outer diameter and 300 mm length, which was vertically positioned and encapsulated in a furnace. To prevent mixing between generated products and quartz wool or catalyst particles escaping from the reactor, products from the reaction flowed past a series of 2- and 5-micron pore-size filters before being condensed in the condenser, whose temperature was maintained at 2 °C by circulating an antifreeze mixture of 40 % water and 60 % by volume of ethylene glycol. This condenser was made of a 316 stainless-steel coil with 3.2 mm outer diameter, 1.8 m length and can recover over 96 wt % of the products as a liquid. The remaining part leaves as gas or stays as a carbon deposit on the catalyst surface.

In each experiment, a support rod was used to enable precise catalyst bed placement. A piece of quartz wool was inserted and flattened on top of the support rod. This flattened piece of quartz wool acted as the bottom of the catalyst bed and prevented any catalyst/reactant from escaping the bed. Then, a mixture of catalyst and PPG, typically 5.0 ± 0.1 g, was added to the reactor and covered with another piece of quartz wool to keep the bed in place, as shown by the red dashed line frame in Fig. 1**a**. To monitor the temperature of the reaction, a thermocouple was introduced into the reactor from the top of the reactor and positioned at about 200 mm above the bottom of the reactor.

### 2.3. Reaction conditions and product analysis

The catalysts were premixed with PPG at a mass ratio of 1:1, the maximum amount of polymer that still resulted in a solid mixed catalyst-polymer bed (see Fig. 1**b**). During the reaction, the concentration of the

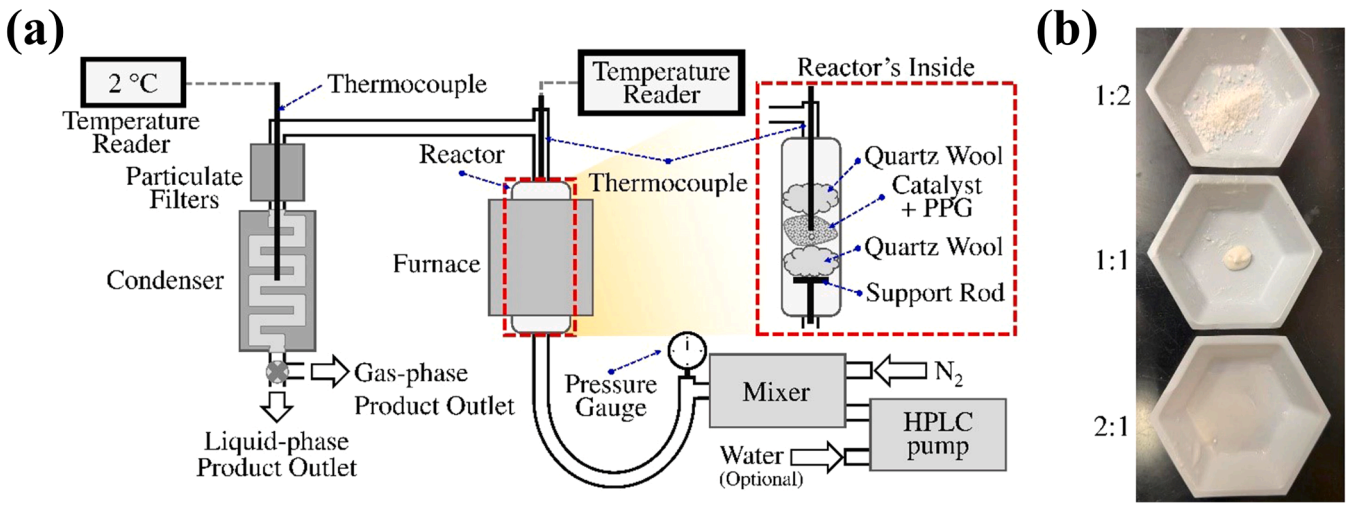


**Fig. 1.** (a) Schematic experimental setup of the system for catalytic cracking of PPG and (b) images of different mass ratios of PPG to catalyst.

reactants decreases, and it changes the catalyst-to-PPG ratio. In other words, during the reaction, the catalyst-to-PPG ratio drops from 1:1 to ~ 1:0. The reaction was carried out under flowing nitrogen at 80 mL/min. First liquid products are collected when the reactor is heated to 450 °C from room temperature. These products are called ramping products. Then, after the setpoint of the reaction was reached, the liquid products were collected every 10 min and were analyzed by gas chromatography-mass spectrometry (GC-MS). After condensation, the exhaust gas was analyzed with a mass spectrometer system with a base pressure of $\sim 10^{-10}$ torr equipped with a Kurt J. Lesker Series 979 vacuum gauge, an MDC ULV-150 leak valve, a Stanford Research Systems RGA 200 mass spectrometer, and a Varian V-250 MacroTorr turbomolecular pump backed by an Alcatel 2021 SD rotary vane pump.

Components of the resulting liquid products were analyzed and identified using a 2010 Shimadzu GC–MS equipped with an RTX-1701 column. The samples were dissolved in a mixture of water and methanol at 50 vol % concentration, and 500 nL of each sample was injected into the column with a split ratio of 30:1. The column temperature was maintained at 40 °C for 3 min. Then, it was increased to 80 °C (2.5 min hold) and to 200 °C (5 min hold) with the same ramp of 20 °C/min. A solvent cut time was implemented to avoid detector saturation from the solvent. The MS scanning was started at 1.35 min from 14 to 380 *m/z* for the remainder of the analysis. In addition, the reactant and products were analyzed by liquid chromatography–mass spectrometry (LC-MS) to calculate the conversion.

The GC–MS can detect more than twenty peaks in the final product mix, which corresponded to five primary products, as follows: (i) propionaldehyde; (ii) 2,5-dimethyl-1,4-dioxane; (iii) 2-ethyl-4-methyl-1,3-dioxolane; (iv) ethyl glycidyl ether; (v) acetone; and (vi) propylene glycol. These products were calibrated using external calibration standards. The selectivity of the products was calculated based on concentrations of the products.

### 2.4. Catalyst characterization

$N_2$ adsorption isotherms were measured at 77 K on a Micromeritics ASAP2020 adsorption instrument with the surface areas and micropore pore volumes determined using the Brunauer–Emmett–Teller (BET) method and mesopore volume determined via the Barrett-Joyner-Halenda (BJH) technique. The acidity of the catalysts was examined by employing temperature-programmed desorption of ammonia ($NH_3$-TPD) using an Anton Paar Autosorb iQ. The samples were treated at 550 °C for 1 h under helium, then exposed to ammonia at 100 °C for 10 min. At the same temperature, non-adsorbed and physisorbed ammonia was removed by helium flow for 30 min. In the next stage, the temperature was increased to 650 °C to desorb ammonia, and flow was monitored using a thermal conductivity detector (TCD).

Solid-state $^{27}$Al MAS NMR spectra of the fresh and spent H-ZSM-5 catalysts were recorded on a Bruker DSX500 spectrometer and a Bruker 4 mm MAS probe. Free induction decay signal was collected after a short rf pulse (0.5 μs-π/18 flip angle) and strong $^{1}$H decoupling pulses in order to characterize isolated tetrahedral framework aluminum and extra-framework aluminum (EFAl) species within the zeolites. The sample spinning rate was 13 kHz at ambient conditions. In addition, $^{13}$C CPMAS NMR was used to investigate the organic residues of PPG on the spent catalyst. Chemical shifts were calibrated externally using 1 M $Al(NO_3)_3$ aqueous solution at 0 ppm for $^{27}$Al nucleus and TMS for $^{13}$C nucleus.

Coking is one of the primary concerns for catalytic cracking reactions [23]. It is the buildup of carbonaceous materials on a catalyst surface and can significantly hinder the performance of a catalyst [23–26]. There are several useful techniques for characterizing coke buildup on post-process catalysts. In this work, TG analysis and PAL spectroscopy were employed.

The spent catalysts were analyzed using a 2010 Shimadzu TGA-50 H with a TA-60WS thermal analysis, a GC-60A flow control unit, and a BLW-50 cooling blower. About 10 mg of the spent catalyst sample was used. The TG analysis was conducted from room temperature to 600 °C at a fixed heating rate of 10 °C/min with a hold of 10 min at 600 °C under air with a fixed flow rate of 200 mL/min. Several tests were performed for each spent catalyst. In addition, transmission electron microscopy (TEM) was performed on fresh and spent H-ZSM-5 (50:1) catalysts using a Hitachi HT7800 Transmission Electron Microscope at 100.0 kV.

PAL measurements of the specimens were carried out with a APV-8702RU spectrometer, TechnoAP spectrometer with a timing resolution of about 170 ps. The PAL spectrometer uses two fast scintillator detectors with $BAF_2$ cylindrical with built-in photomultiplier tubes H3378–51 manufactured by Hamamatsu Photonics. The Na-22 radioactive source, with a half-life of 2.6 years, serves as a positron generator with examined samples in the sandwich arrangement. The Na-22 source emits positron in coincidence with high energy γ-rays with the energy of 1.27 MeV. The high energy gamma signal is employed as a “start” for opening the timing gate, while the positron annihilation event is marked by detecting one of 511 keV gamma peaks from the annihilation of positrons, and the electron records the “stop”. The sealed source was produced by Eckert & Ziegler Isotope Products, with an activity of 50 mCi (1.85 MBq) on Dec. 4, 2019. It is a disk with an active diameter of 9.83 mm (9.275") enclosed in thin titanium layers of 0.0005" diameter.

## 3. Results and discussion

### 3.1. Thermal decomposition of PPG

The non-catalytic thermal decomposition of PPG starts at around 350 °C [27], i.e., around the reaction temperatures applied here. Therefore, it was necessary to study the product distribution of the thermal decomposition (i.e., in the absence of a catalyst) in order to be able to elucidate the contribution of the catalyst. To assess the thermal decomposition characteristics of PPG, it was thoroughly mixed with sand, and then the reaction was conducted at 450 °C for 1 h to achieve complete conversion. The product distribution of the thermal decomposition of PPG is presented in Table 1. Acetone and propionaldehyde are the dominant products under the given reaction conditions, though, as typical for thermal cracking, there are at least 5 chemical products being synthesized in more than 7 % selectivity. In summary, it was found that the product distribution of non-catalytic thermal decomposition of PPG is not selective enough for value-added upcycling.

### 3.2. Catalytic upcycling of PPG

Because the thermal decomposition of PPG shows only a maximum selectivity of around 30 % towards propionaldehyde – as the primary product, we began investigating catalytic approaches that could increase this selectivity towards this product. For example, by adding H-ZSM-5 with $SiO_2/Al_2O_3$ ratios of 23:1 and 50:1, the catalytic reaction at 450 °C reached complete conversion within 30 min, as evidenced by the lack of reaction products in the reactor effluent and the lack of reactant on the catalyst. The reactor effluent was analyzed by LC-MS, GC-MS, and

**Table 1**
Main products during the thermal (non-catalytic) decomposition of PPG at 450 °C for 1 h under nitrogen flow.

| Product name | Selectivity (%) |
|---|---|
| Ethanol | 2.98 |
| Propionaldehyde | 32.28 |
| Acetone | 24.68 |
| Isopropyl alcohol | 7.44 |
| 1-Propanol | 2.02 |
| 2,2,4-Trimethyl- 1,3-dioxlane | 7.21 |
| 1,2-Ethanediol | 11.67 |
| Others | 11.73 |

MS; in addition, the spent catalysts were analyzed by $^{13}C$ MAS NMR. This result demonstrates that in the presence of catalyst, the reaction could reach full conversion faster than the non-catalytic reaction. Mass measurements of the reaction products showed that 95–96 wt % of the products were collected as a liquid, and between 1 and 3 wt % of the products were deposited onto the surface of the catalyst as a solid residue, depending primarily on the acidity of the zeolite. The percentage of the solid products was analyzed by TG analysis. The remaining part (~ 2 %) of the products leaves the reactor as a gas, which was analyzed by MS. The gas products mainly consisted of hydrogen and carbon monoxide. In addition, small amounts of carbon dioxide and propylene oxide were detected. Small amounts of other hydrocarbon fragments were alsoverified, but were difficult to analyze in detail. Fig. 2 shows the liquid product distribution/selectivity collected after 20 min (including ramping time) driven from catalytic cracking of PPG over H-ZSM-5 catalyst with a $SiO_2/Al_2O_3$ ratio of 50:1, as a function of reaction temperature. From this figure, the selectivity towards propionaldehyde is significantly enhanced if compared to the results of thermal decomposition. Even at a relatively low reaction temperature of 350 °C, the selectivity doubles with the catalyst present. By increasing the reaction temperature from 350° to 450°C, a selectivity close to 80 % toward propionaldehyde can be reached.

However, further raising the reaction temperature to 550 °C would not markedly influence the product distribution in the liquid phase. An inverse trend can be observed for the selectivity towards 4,5-dimetyl-1,3-dioxane relative to propionaldehyde. Previously, it was reported that 4,5-dimetyl-1,3-dioxane mainly formed at room temperature [28] and that Lewis acid sites play a vital role in the production of dioxanes [29]. At lower reaction temperatures, ethyl glycidyl ether also had higher concentrations in the product liquid, but its formation almost completely disappeared at 450 °C or higher temperatures. This phenomenon can be rationalized based on the known limited thermal stability of glycidyl ethers [34], which is in contrast to propionaldehyde's stability even at 450 °C under inert gas in the absence of oxygen [30]. In summary, we found that the highest selectivity to a single product, propionaldehyde, during PPG cracking at a temperature of 450 °C.

To investigate the effect of the water content in the feed on the reaction, a series of experiments were conducted under steam with different flow rates of 20–100 mL/min. Selectivity results as a function of flow rate are given in Fig. 3. A gradual decrease in the selectivity towards propionaldehyde was observed for higher steam flow rates. The selectivity toward 2-ethyl-4-methyl-1,3-dioxolane and propylene glycol increased with increasing steam flow, while 4,5-dimethyl-1,3-dioxane decreased. This result indicated that the concentration of steam could significantly affect the activity of the catalyst. Typically, steam may cause two effects on the catalytic activity: (i) Steam can act as a reactant and cause the production of byproducts. (ii) Steam can adsorb on the zeolite, inhibiting specific active sites and causing dealumination [31]. In the case of the latter, it is critical to note that the presence of steam can have a strong effect on the structure of the zeolite-based catalysts at high temperatures [32], which can also cause a substantial effect on the catalytic efficiency of the zeolites [43–45].

It has been demonstrated that a higher acidity of a zeolite can markedly affect its catalytic activity [33–35]. Nevertheless, the enhancement of the number of active sites does not always lead to a higher selectivity toward the desired products [34]. Fig. 3 also displays the selectivity for the main products from the catalytic cracking of PPG using the H-ZSM-5 catalyst with a $SiO_2/Al_2O_3$ ratio of 23:1 under nitrogen. These data demonstrate that the selectivity of H-ZSM-5 (23:1) towards propionaldehyde is about 10 % lower than that of H-ZSM-5 (50:1). To have better understanding the difference between the selectivity between the H-ZSM-5-based catalysts, several complementary characterization techniques were employed in this study, as described in the following section.

### 3.3. Structural properties

The $N_2$ adsorption–desorption isotherms for the two zeolite samples are shown in Fig. S1. The calculated surface areas and corresponding pore volumes are tabulated in Table 2. These data demonstrate that H-ZSM-5 (50:1) has a higher mesopore volume, which is mainly due to having less interlayer interaction compared to H-ZSM-5 (23:1). From the results previously reported in the literature, more aluminum causes more interlayer interaction, which results in less porosity of the zeolites [36]. As can be found from Table 1, some reaction is also taking place without the catalyst. In this case, a decreasing mesopore volume and surface area cause an increase in the non-catalytic part of the reaction, as PPG has a large molecule size and therefore requires wider pores to interact with the surface of the catalyst. Importantly, the pore size of the ZSM-5 framework is around 0.5 nm, while the molecular size of a propylene glycol is also around 0.5 nm [37–39]. In this study, PPG with a molecular weight of 425 was used, which has an average of 5–6 propylene molecules and is expected to be significantly larger than the pore size of the ZSM-5 framework. As shown in Fig. 3, selectivity towards acetone and propylene glycol was increased in the lower mesopore volume and surface area. Acetone and propylene glycol are significant products of non-catalytic reactions, as given in Table 1. Therefore, increasing selectivity towards some byproducts can be explained by the lack of interaction between the active surface of the catalyst and PPG in the presence of a catalyst with a lower mesopore surface area. This is in line with previous studies, which correlated mesopore surface area and cracking rates of polymers [40,41]. However, we cannot rule out the possibility that the nature of the acid sites is also different in these two catalysts, concerning a potentially different Lewis-to-Bronsted acid-site

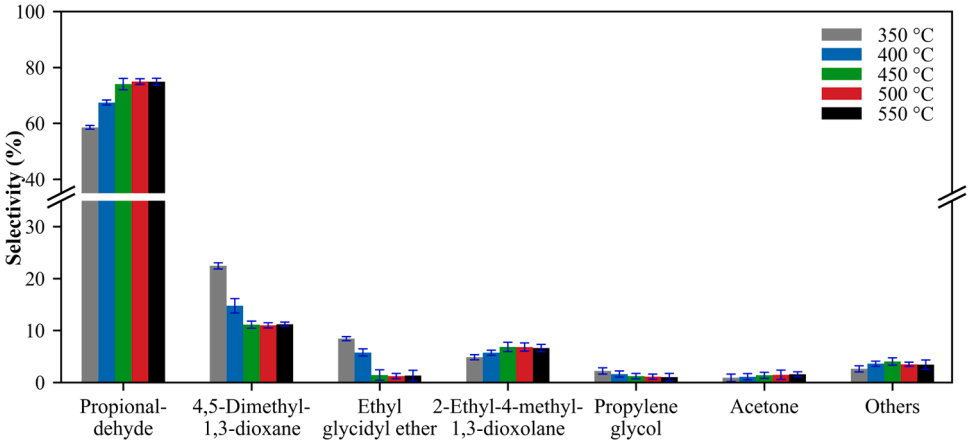


**Fig. 2.** Effect of temperature on selectivity of primary products. (Reaction conditions: catalyst: H-ZSM-5 (50:1), catalyst/PPG ratio: 1/1, under nitrogen flow.).

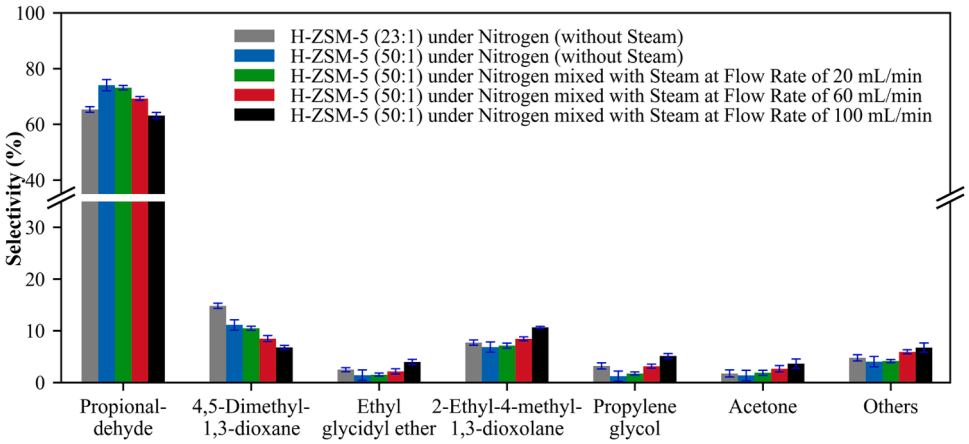


**Fig. 3.** Selectivity for main products with and without steam for the H-ZSM-5 (50:1), as well as without steam for the H-ZSM-5 (23:1) at 450 °C.

**Table 2**
Pore volume and surface area of H-ZSM-5 with $SiO_2/Al_2O_3$ ratios of 23:1 and 50:1.

| Sample | BET SA ($m^2/g$) | Micro SA ($m^2/g$) | Meso SA ($m^2/g$) | Micro PV ($cm^3/g$) | Meso PV ($cm^3/g$) |
|---|---|---|---|---|---|
| H-ZSM-5 (23:1) | 420 | 279 | 141 | 0.133 | 0.106 |
| H-ZSM-5 (50:1) | 443 | 248 | 195 | 0.101 | 0.144 |

ratio and acid-site strengths, as well as differing amounts of extra-framework Al species. These effects are described below in more detail.

$NH_3$-TPD was used to assess the presence and the relative amount of acid sites on the zeolites. As depicted in Fig. 4, the H-ZSM-5 (23:1) exhibited a nearly two times higher total acid site concentration than H-ZSM-5 (50:1), which can be attributed to the aluminum-based acidic sites on the zeolites [44]. The lower and higher temperature peaks in the TPD spectra can be assigned to the weakly and strongly bonded ammonia on the catalyst's surface, respectively, corresponding to strong and weak acidic sites [42]. It can also be observed that the centers of the individual peaks are not located at the same temperature. The strength of the acidic sites on H-ZSM-5 (23:1) is slightly higher than on the H-ZSM-5 (50:1), which is indicated by a shift of the first desorption peak center from 178° to 198°C, as well as a shift of the second desorption peak center from 378° to 398°C. These results demonstrate the difference in the nature of the active sites on the surface of the H-ZSM-5

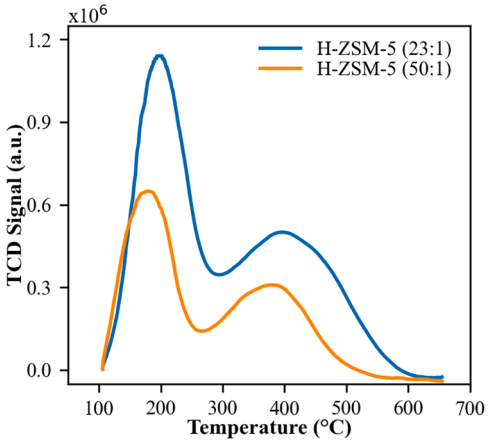


**Fig. 4.** $NH_3$-TPD results of the fresh H-ZSM-5 catalysts.

samples with different $SiO_2/Al_2O_3$ ratios, which leads to differences in their catalytic activity toward the decomposition of PPG. It is essential to mention that the actual catalytic process is complex, including pathways that are in the fluid phase coupled with processes on the external acid sites (for initial cracking) as well as subsequent creation of intermediates on internal acid sites. In this context, further characterization of the difference in types of active sites will be discussed in the next paragraph.

$^{27}Al$ MAS NMR spectra of the fresh and used catalysts were compared in Fig. 5. In this figure, three different spectral regions provide information about aluminum coordination number and connectivity in the zeolite framework. The peaks centered around 0 and 55 ppm can be attributed to the octahedral and tetrahedrally coordinated Al in the crystal structure of the sample [43]. The shoulder only observed for the spent H-ZSM-5 (23:1) sample centered around 30 ppm represents penta-coordinated aluminum [44]. These changes in H-ZSM-5 (23:1) may lead to noticeable differences in the activity of this catalyst. The absence of the shoulder for the H-ZSM-5 (50:1) may suggest that the structure remains stable after the reaction. The peak at 0 ppm, as shown in Fig. 5, demonstrates that H-ZSM-5 (23:1) possesses more EFAl. At the same time, only a very small peak can be detected for H-ZSM-5 (50:1), corresponding to extra-framework Al. The substantial differences in the activity of the H-ZSM-5 (23:1) and H-ZSM-5 (50:1) can be related to the number of EFAl sites on the surface of H-ZSM-5 samples. This type of aluminum coordination is expected to increase the contribution of Lewis-acidic sites on the surface of the catalysts [45]. As previously reported in the literature [48,49], 1,3-dioxolane and 1,4-dioxane rings can be preferentially formed from oxiranes in the presence of Lewis-acidic sites [48,49]. The catalytic activity of the H-ZSM-5 (23:1) with EFAl follows a similar trend that leads to an increase in the selectivity for 2-ethyl-4-methyl-1,3-dioxolane and 4,5-dimethyl-1,3-dioxane.

Spent catalysts were also evaluated using TG analysis to assess coke formation or the presence of other organic residues on the surface of different samples. From the obtained results (see Fig. 6), it was found that the H-ZSM-5 (23:1) and H-ZSM-5 (50:1) lost about 2.39 ± 0.06 wt % and 1.39 ± 0.03 wt %, respectively, of their initial weights. These results can be attributed to the nature of Al content of the zeolite samples, which is associated with a higher concentration of strong acid and extra framework/Lewis-acidic sites. Regarding the $NH_3$-TPD results (Fig. 4), the H-ZSM-5 (23:1) sample exhibits a higher number of acidic sites compared with H-ZSM-5 (50:1), which was mainly correlated to the aluminum content of zeolites [46,47]. On the other hand, the confirmed mass losses can be originated from the burning of coke that formed during the catalytic cracking procedure. Further proof of this hypothesis was obtained by $^{13}C$ MAS NMR on the spent H-ZSM-5 (50:1) catalyst, as shown in Fig. 7. The spectra showed the existence of condensed aromatics and coke on the sample's surface, which is typically reported after reactions of zeolite-based catalysts with hydrocarbons [48].

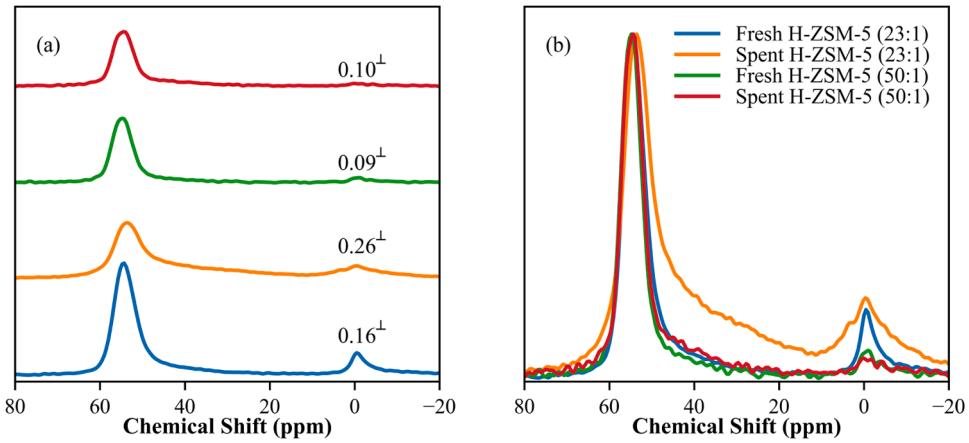


**Fig. 5.** (a) Raw $^{27}$Al MAS NMR measurements of H-ZSM-5 catalysts by varying $SiO_2/Al_2O_3$ ratio, measured before and after catalytic reaction, and (b) normalized $^{27}$Al MAS NMR measurements to isolated tetrahedral Al species at ~ 60 ppm. Note that $^{\perp}$ refers to the ratio of EFAl species compared to the total Al.

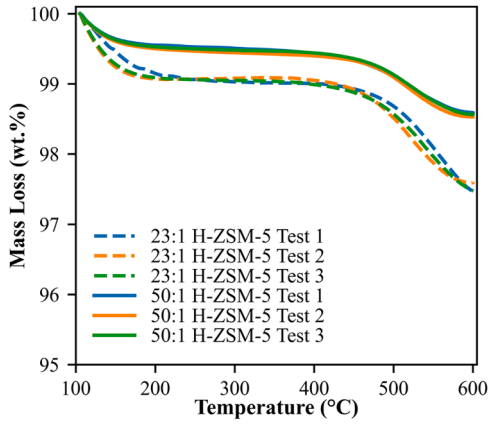


**Fig. 6.** TG analysis of spent H-ZSM-5 catalysts with two different $SiO_2/Al_2O_3$ ratios (23:1 and 50:1).

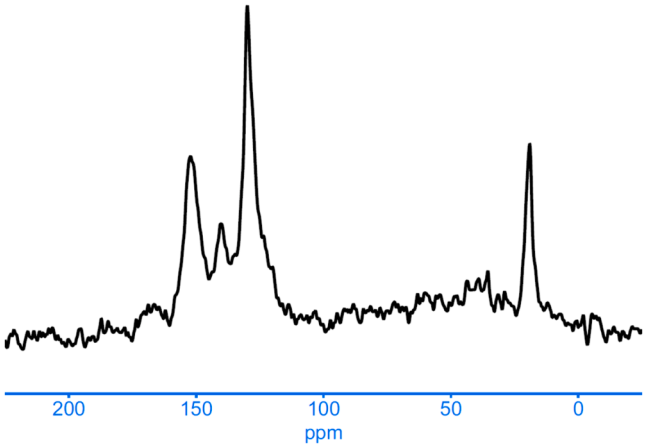


**Fig. 7.** $^{13}$C MAS NMR results of spent H-ZSM-5 (50:1).

Fig. 8 displays TEM images of fresh and spent H-ZSM-5 (50:1) catalysts. The results show that the spent catalysts kept their crystalline shape and have clear edges. Fig. 8**c** further indicates a small amount of coke on the surface of the catalyst, which was previously confirmed by $^{13}$C MAS NMR, TGA, and PALS results.

### 3.4. PALS analysis

PALS was employed to analyze nanostructure and morphology, including voids, vacancies, defects, and microporous structures and respective concentrations, of catalysts before and after being used in catalytic cracking of PPG. In metals, positrons annihilate either from the bulk non-localized state (with a lifetime at 100–150 ps) or from the trapped state. The lifetime of the trapped state is higher due to lower electron density, at about 200–500 ps, depending on the type of trap. In non-conductive materials with high nano- and micro-porosities and free volumes (such as polymers, silica-gels, and zeolites) positrons can localize as a positron-electron hydrogen-like atom, called positronium. A positronium in the para-state (opposite spins for electron and positron) decays with a lifetime of 125 ps. Still, a positronium in the ortho-state, o-Ps, with parallel spins decays in a time over 1 ns. A positronium is created in the o-Ps state three out of four times, contributing to long lifetimes. Positroniums live much longer than “free” or “trapped” positrons. The self o-Ps annihilation lifetime (in vacuum) is 142 ns, 1000 times more than for positrons in bulk. Usually, o-Ps decay in a shorter time with the neighboring electron rather than its own with parallel spin; this effect is called o-Ps pick-off. This allows for a far more in-depth analysis of pore size and the fraction of microporous structures since o-Ps lifetime is related to the pore size and its intensity to the free volume fraction. In the present work, fresh and spent H-ZSM-5 samples were analyzed by PALS. PALS analysis of the pelletized samples was carried out using LT v9.2 Kansy software [49] in two different timing ranges for a better understanding of positronium effects. The range of short timing goes to about 60 ns, the long one over 200 ns, so the short range is the most sensitive towards lifetimes less than 2 ns long. In contrast, the long lifetime is better for longer lifetimes related to the micro-pore size of positronium.

The PALS analysis was performed to examine the nano and meso-porosity of the fresh H-ZSM-5 catalysts and investigate the blocking of pores and active sites for spent samples. As presented in Table 3, PAL data are distributed into three discrete lifetimes, which are related to annihilation in bulk ($T_1$), positron trapping ($T_2$), and positronium formation ($T_3$) with their appropriate weights (intensities). The longest lifetime and intensity are mainly assigned to the open-volume micro- and meso-porous structures. Regarding this table, a large change in the lifetimes and intensity values for spent catalysts can be found after the reaction. Accordingly, the $I_3$ of H-ZSM-5 (23:1) decreased from 14.9 % for fresh to 5.30 % for spent sample, along with a decrease in the lifetime from 2.799 ns (fresh) to 2.123 ns (spent). This result demonstrates a significant alteration in the morphological structure caused by the conversion and coking of zeolite samples. For H-ZSM-5 (50:1) sample, coking can cause a significant change. However, the fresh zeolite

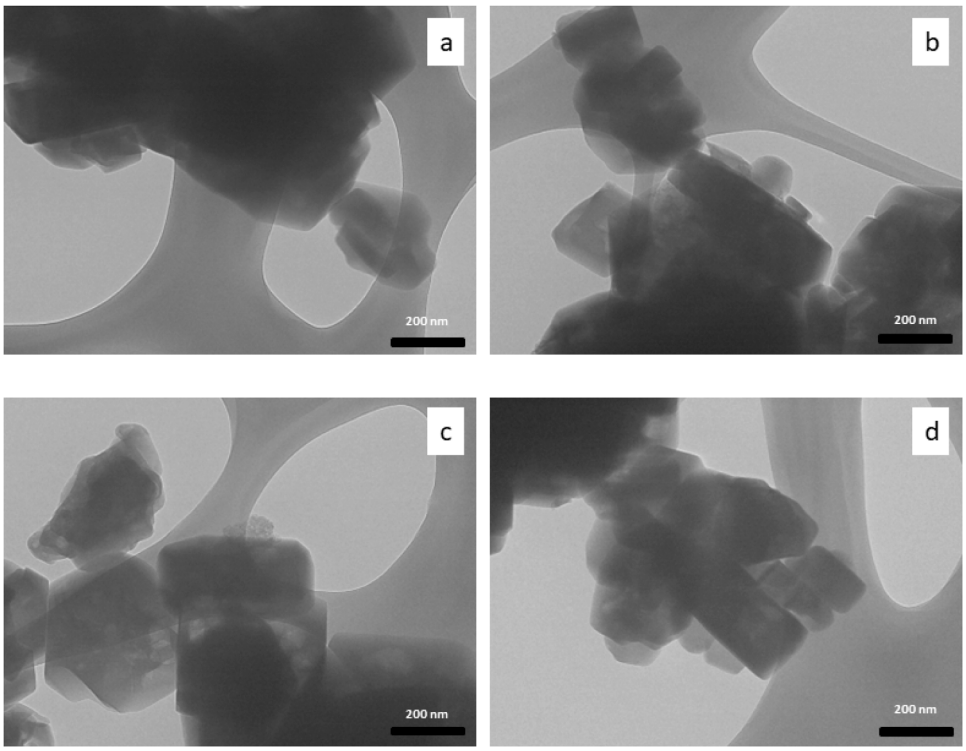


**Fig. 8.** TEM images of (a, b) fresh and (c, d) spent of H-ZSM-5 (50:1) samples.

**Table 3**
PALS results and standard deviation for the four H-ZSM-5 samples with source correction.

| Sample | $T_1$ | $I_1$ | $T_2$ | $I_2$ | $T_3$ | $I_3$ | T total |
|---|---|---|---|---|---|---|---|
| Fresh H-ZSM-5 (23:1) | 0.159 | 40.69 | 0.499 | 44.40 | 2.799 | 14.92 | 70.38 |
| Spent H-ZSM-5 (23:1) | 0.159 | 35.47 | 0.466 | 59.23 | 2.123 | 5.30 | 44.53 |
| Fresh H-ZSM-5 (50:1) | 0.165 | 37.74 | 0.510 | 56.88 | 2.885 | 5.38 | 50.53 |
| Spent H-ZSM-5 (50:1) | 0.159 | 33.84 | 0.480 | 63.45 | 2.163 | 2.71 | 41.69 |

exhibits less stoichiometric mismatch to start with since the initial intensity, $I_3$, was only 5.38 %. Besides, its lifetime ($I_3$) was longer at 2.885 ns, suggesting the presence of larger pore sizes in the initial stage of the process. Importantly, the intensity was suppressed from 5.28 % to 2.71 % by changing the lifetime from 2.885 ns to 2.163 ns. There is a significant change in the morphology of the H-ZSM-5 (23:1) samples, as it was discussed for the NMR results and depicted in Fig. 5.

Moreover, there is a change in the positron trapping signal after the reaction by decreasing the trapping lifetime ($T_2$), while its intensity is increased. This phenomenon can be linked to the loss of the available free volume during catalysis, which causes a collapse or division of meso- and nano-pore structures. In general, by enhancing the nano-porosity, too small for a positronium to be localized but sufficient for positron trapping to occur [49].

Due to the PALS analysis being conducted for two different timing regions, the lifetimes were distributed onto two long-range regions for long-timing range measurements. This analysis demonstrated that fresh H-ZSM-5 (50:1) has a higher fraction of meso-porosity compared with H-ZSM-5 (23:1). Meanwhile, H-ZSM-5 (23:1) exhibited a higher fraction of micro-porosity comparing to the H-ZSM-5 (50:1). It is worth to mention that the fraction of meso-pores was relatively small, not exceeding 1 % of the total positron processes. Still, it was far enough from the shorter lifetimes.

### 3.5. Possible reaction pathways

Fig. 9 depicts a possible pathway for cracking of PPG in the presence and absence of catalysts. Although the exact mechanism of the process is not fully developed, a discussion of the reaction is given by combining the obtained results in this study and previous reports [50]. By focusing on the chemical structure of the six main products, they can be categorized into two distinct groups: (i) three- and (ii) six-carbon atoms products. Due to the repeating unit of the PPG reactant composed of three carbon atoms and considering the product distribution, it can be postulated that the reaction has intermediates that consist of three carbon atoms. During product analysis, a minimal amount of propylene oxide (PO) was detected. However, PO is unstable at high temperatures (350–550 °C) and usually converts to propionaldehyde, acetone, and other products [27]. By considering the product distribution, PO, acetone, and propionaldehyde are the three-carbon molecules that can play as an intermediate to synthesize other six-carbon or larger molecule products. In addition, 2,5-dimethyl-1,4-dioxane and 2-ethyl-4-methyl-1, 3-dioxolane have a ring-like chemical structure, which is precisely two times of the atomic elements of acetone and propionaldehyde with a double-bonded oxygen atom. It was hypothesized that the repeating unit of PPG can be directly converted into acetone by forming a double bond between carbon and oxygen and rearranging the hydrogen atoms. Although this conversion may be only restricted to pyrolytic cracking reactions of PPG, the high selectivity of acetone was verified during the thermal cracking reaction. In contrast, a low selectivity of acetone was observed, as can be found in Table 1 and Figs. 2 and 3. Considering the products, it is observed that all products can, in principle, be synthesized from PO. To confirm this postulate, pure PO was used as a reactant instead of PPG, and the same products were detected in the liquid product mixture. This is well-matched with a previous study of thermal conversion of mono-propylene glycol via dehydration that PO intermediate was formed before conversion to propionaldehyde and acetone [51]. Likewise, it may also be possible to directly convert those units

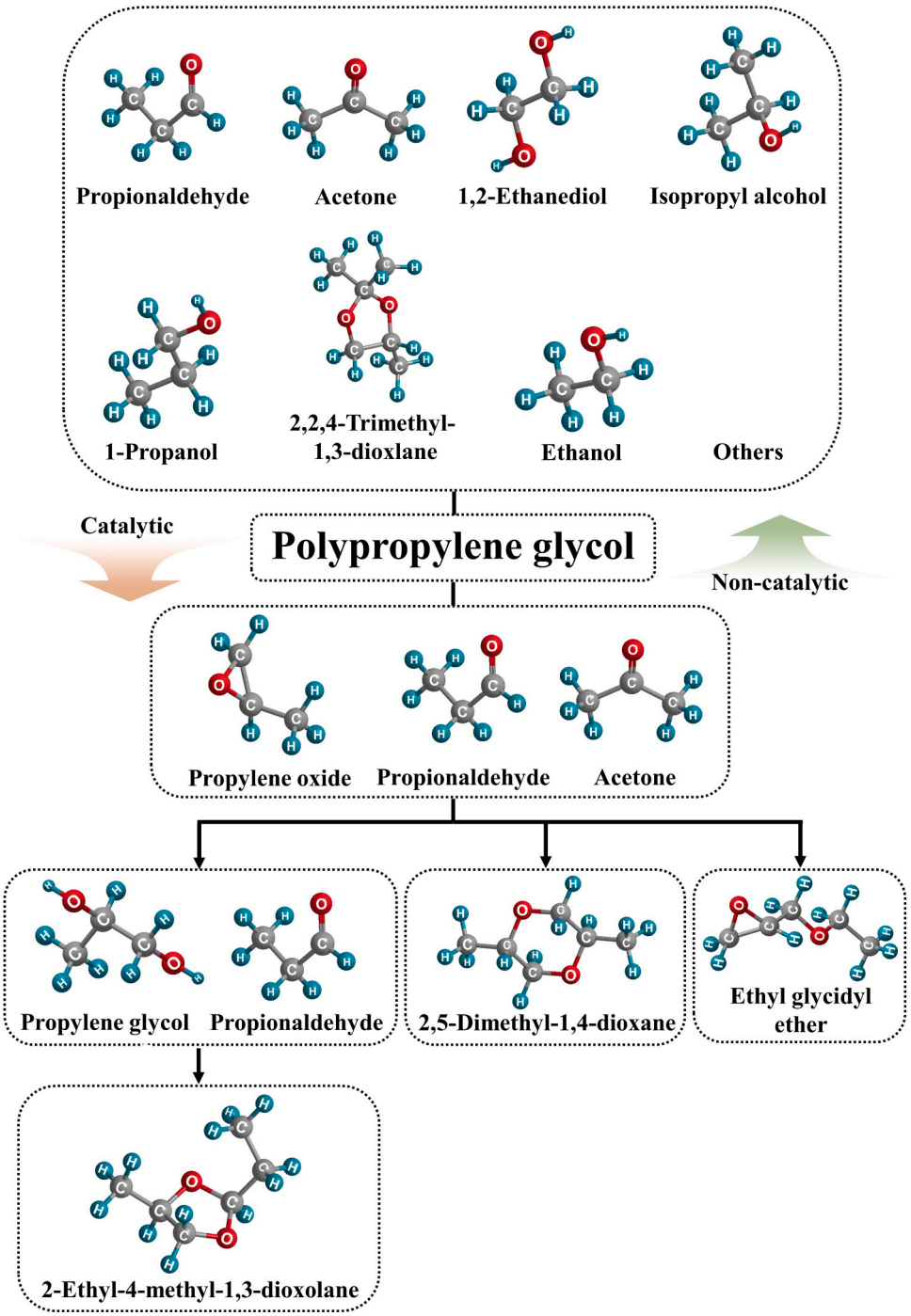


**Fig. 9.** Proposed reaction mechanisms of catalytic and non-catalytic cracking of PPG.

into propionaldehyde with a regioselective reaction, such as hydroformylation [52–57]. Interestingly, propylene glycol can be synthesized from PO in the presence of steam [58], and a similar trend was detected in the reaction by increasing steam concentrations and enhancing the selectivity of propylene glycol (Fig. 3).

Moreover, it is possible to produce 2-ethyl-4-methyl-1,3-dioxolane and water from propylene glycol and propionaldehyde in the presence of an acidic catalyst [59]. Another main byproduct, 2,5-dimethyl-1,4-dioxane, can be generated from PO over H-ZSM-5 and Cu-ZSM-5 [60]. Similar trends may occur with other three-carbon oxygen--containing intermediates, including acetone or propionaldehyde. Acetone and propionaldehyde can be synthesized from PO in the presence of acidic sites. Isomerization of PO is well-accepted and shows the synthesis of acetone, propionaldehyde, allyl alcohol, and other products through this reaction [61]. Another byproduct is ethyl glycidyl ether which is reported as a derivative of PPG by different research groups [62]. There are different possible pathways to synthesize the ethyl glycidyl ether from PPG; however, in this study, it is postulated that it can be formed using a reaction between propionaldehyde and PO.

Changes in reaction bed configuration, residence time, and reaction parameters affect the selectivity significantly. Whenever the residence time is long, the products may react again on the catalyst surface. In this study, it is observed that with different bed configurations and residence times, benzene, toluene, and xylene can be produced from the PPG. This process can easily be scaled-up in fluidized bed reactors. However, reaction conditions should be optimized again to get high selectivity of

propionaldehyde.

## 4. Conclusion

PPG was used as a model of oxygenated polymer and catalytically decomposed to six primary products, including (i) propionaldehyde; (ii) 2,5-dimethyl-1,4-dioxane; (iii) 2-ethyl-4-methyl-1,3-dioxolane; (vi) acetone; (v) ethyl glycidyl ether; and (vi) propylene glycol. Commercial H-ZSM-5 catalysts with silica-to-alumina ratios of 23:1 and 50:1 were employed in the reaction. Both zeolites have the same framework structure and were tested in the hydrogen form, but they showed significantly different activity during the reaction. It is observed that the main differences between the tested zeolites were the amount of extra-framework aluminum and different concentration and strength of active sites. H-ZSM-5 (23:1) had higher extra-framework aluminum and a higher total amount of active sites. It showed lower selectivity to propionaldehyde (69.71 %) in the liquid product. H-ZSM-5 (50:1) exhibited 74.41 % selectivity to propionaldehyde. PALS demonstrated that the structure of H-ZSM-5 was altered slowly in the PPG reaction, whereas extra framework aluminum of 23:1 H-ZSM-5 was not stable for the reaction.

## CRediT authorship contribution statement

**Kanan Shikhaliyev:** Investigation, Writing - Original Draft, Writing - Review & Editing, **Thossaporn Onsree:** Investigation, Writing - Original Draft, Writing - Review & Editing, **Andrew H. Jaeschke:** Investigation, Writing - Original Draft, **Seyed Majid Ghoreishian:** Writing - Review & Editing, **Kaveh Shariati:** Investigation, **Abraham Martinez:** Investigation, Writing - Original Draft, **Alexander Katz:** Conceptualization, Supervision, Project administration, **Sonjong Hwang:** Investigation, **Anne Gaffney:** Supervision, **Jagoda M. Urban-Klaehn:** Investigation, Writing - Original Draft, **Jochen Lauterbach:** Conceptualization, Supervision, Project administration, Funding acquisition.

## Declaration of Competing Interest

The authors declare the following financial interests/personal relationships which may be considered as potential competing interests: Jochen Lauterbach reports financial support was provided by National Science Foundation.

## Data availability

Data will be made available on request.

## Acknowledgment

The authors acknowledge funding from the US National Science Foundation grant NSF IIP 1939876.

## Appendix A. Supporting information

Supplementary data associated with this article can be found in the online version at doi:10.1016/j.apcatb.2023.122991.

## References

[1] L.S.T.J. Korley, T.H. Epps, B.A. Helms, A.J. Ryan, Toward polymer upcycling-adding value and tackling circularity, Science 373 (2021) 66–69, https://doi.org/10.1126/science.abg4503.
[2] C. Wang, H. Han, Y. Wu, D. Astruc, Nanocatalyzed upcycling of the plastic wastes for a circular economy, Coord. Chem. Rev. 458 (2022), 214422, https://doi.org/10.1016/J.CCR.2022.214422.
[3] J.N. Hahladakis, E. Iacovidou, S. Gerassimidou, Plastic waste in a circular economy, Plast. Waste Recycl. (2020) 481–512, https://doi.org/10.1016/B978-0-12-817880-5.00019-0.
[4] R. Geyer, J.R. Jambeck, K.L. Law, Production, use, and fate of all plastics ever made, Sci. Adv. 3 (2017), https://doi.org/10.1126/sciadv.1700782.
[5] J.M. Garcia, M.L. Robertson, The future of plastics recycling, Science 358 (2017) 870–872, https://doi.org/10.1126/science.aaq0324.
[6] M.A. Garrido, R. Font, Pyrolysis and combustion study of flexible polyurethane foam, J. Anal. Appl. Pyrolysis 113 (2015) 202–215, https://doi.org/10.1016/J.JAAP.2014.12.017.
[7] A.S. Dutta, Polyurethane foam chemistry, Recycl. Polyurethane Foams (2018) 17–27, https://doi.org/10.1016/B978-0-323-51133-9.00002-4.
[8] J.L. Blevins, K. Martinez, A political-economic history of FCC policy on minority broadcast ownership. https://doi.org/10.1080/10714421.2010.502806.
[9] E.T.C. Vogt, B.M. Weckhuysen, Fluid catalytic cracking: recent developments on the grand old lady of zeolite catalysis, Chem. Soc. Rev. 44 (2015) 7342–7370, https://doi.org/10.1039/C5CS00376H.
[10] J. Biswas, I.E. Maxwell, Recent process- and catalyst-related developments in fluid catalytic cracking, Appl. Catal. 63 (1990) 197–258, https://doi.org/10.1016/S0166-9834(00)81716-9.
[11] J.N. Armor, New catalytic technology commercialized in the USA during the 1980′s, Appl. Catal. 78 (1991) 141–173, https://doi.org/10.1016/0166-9834(91)80103-4.
[12] E.T.C. Vogt, G.T. Whiting, A. Dutta Chowdhury, B.M. Weckhuysen, Zeolites and zeotypes for oil and gas conversion, Adv. Catal. 58 (2015) 143–314, https://doi.org/10.1016/BS.ACAT.2015.10.001.
[13] S.L. Wong, N. Ngadi, T.A.T. Abdullah, I.M. Inuwa, Current state and future prospects of plastic waste as source of fuel: a review, Renew. Sustain. Energy Rev. 50 (2015) 1167–1180, https://doi.org/10.1016/J.RSER.2015.04.063.
[14] A. López, I. de Marco, B.M. Caballero, A. Adrados, M.F. Laresgoiti, Deactivation and regeneration of ZSM-5 zeolite in catalytic pyrolysis of plastic wastes, Waste Manag. 31 (2011) 1852–1858, https://doi.org/10.1016/J.WASMAN.2011.04.004.
[15] A.G. Buekens, H. Huang, Catalytic plastics cracking for recovery of gasoline-range hydrocarbons from municipal plastic wastes, Resour. Conserv. Recycl. 23 (1998) 163–181, https://doi.org/10.1016/S0921-3449(98)00025-1.
[16] E. Rodríguez, A. Gutiérrez, R. Palos, F.J. Vela, J.M. Arandes, J. Bilbao, Fuel production by cracking of polyolefins pyrolysis waxes under fluid catalytic cracking (FCC) operating conditions, Waste Manag. 93 (2019) 162–172, https://doi.org/10.1016/J.WASMAN.2019.05.005.
[17] A. de, R. Pinho, M.B.B. de Almeida, F.L. Mendes, L.C. Casavechia, M.S. Talmadge, C.M. Kinchin, H.L. Chum, Fast pyrolysis oil from pinewood chips co-processing with vacuum gas oil in an FCC unit for second generation fuel production, Fuel 188 (2017) 462–473, https://doi.org/10.1016/J.FUEL.2016.10.032.
[18] C. Xing, G. Yang, M. Wu, R. Yang, L. Tan, P. Zhu, Q. Wei, J. Li, J. Mao, Y. Yoneyama, N. Tsubaki, Hierarchical zeolite Y supported cobalt bifunctional catalyst for facilely tuning the product distribution of Fischer–Tropsch synthesis, Fuel 148 (2015) 48–57, https://doi.org/10.1016/J.FUEL.2015.01.040.
[19] S. Sartipi, K. Parashar, M.J. Valero-Romero, V.P. Santos, B. Van Der Linden, M. Makkee, F. Kapteijn, J. Gascon, Hierarchical H-ZSM-5-supported cobalt for the direct synthesis of gasoline-range hydrocarbons from syngas: Advantages, limitations, and mechanistic insight, J. Catal. 305 (2013) 179–190, https://doi.org/10.1016/J.JCAT.2013.05.012.
[20] M.F. Ali, M.N. Siddiqui, Thermal and catalytic decomposition behavior of PVC mixed plastic waste with petroleum residue, J. Anal. Appl. Pyrolysis 74 (2005) 282–289, https://doi.org/10.1016/J.JAAP.2004.12.010.
[21] S.L. Wong, N. Ngadi, T.A.T. Abdullah, I.M. Inuwa, Current state and future prospects of plastic waste as source of fuel: A review, Renew. Sustain. Energy Rev. 50 (2015) 1167–1180, https://doi.org/10.1016/j.rser.2015.04.063.
[22] Process for treating polyether polyols, (1994).
[23] E.E. Wolf, F. Alfani, Catalysts deactivation by coking, Catal. Rev. 24 (2007) 329–371, https://doi.org/10.1080/03602458208079657.
[24] A. Durmuş, S.N. Koç, G.S. Pozan, A. Kaşgöz, Thermal-catalytic degradation kinetics of polypropylene over BEA, ZSM-5 and MOR zeolites, Appl. Catal. B 61 (2005) 316–322, https://doi.org/10.1016/J.APCATB.2005.06.009.
[25] C. Wang, H. Lei, Y. Zhao, M. Qian, X. Kong, W. Mateo, R. Zou, R. Ruan, Integrated harvest of phenolic monomers and hydrogen through catalytic pyrolysis of biomass over nanocellulose derived biochar catalyst, Bioresour. Technol. 320 (2021), 124352, https://doi.org/10.1016/J.BIORTECH.2020.124352.
[26] S. Kim, E. Sasmaz, J. Lauterbach, Effect of Pt and Gd on coke formation and regeneration during JP-8 cracking over ZSM-5 catalysts, Appl. Catal. B 168–169 (2015) 212–219, https://doi.org/10.1016/J.APCATB.2014.12.027.
[27] L.X. Song, X.Q. Guo, F.Y. Du, L. Bai, Thermal degradation comparison of polypropylene glycol and its complex with β-cyclodextrin, Polym. Degrad. Stab. 95 (2010) 508–515, https://doi.org/10.1016/j.polymdegradstab.2009.12.025.
[28] H. Firouzabadi, N. Iranpoor, B. Karimi, Zirconium tetrachloride ($ZrCl_4$) catalyzed highly chemoselective and efficient transthioacetalization of acetals, Synlett 4 (1999) 319–320, https://doi.org/10.1055/s-1999-2609.
[29] B. Karimi, G.R. Ebrahimian, H. Seradj, Efficient and chemoselective conversion of carbonyl compounds to 1,3-dioxanes catalyzed with N-bromosuccinimide under almost neutral reaction conditions, Org. Lett. 1 (1999) 1737–1739, https://doi.org/10.1021/ol9909987.
[30] A. Hensel, Propanal, Ullmann's Encyclopedia of Industrial Chemistry, John Wiley & Sons, Ltd, 2018, pp. 1–8, https://doi.org/10.1002/14356007.a22_157.pub3.
[31] C.J. Baranowski, T. Fovanna, M. Roger, M. Signorile, J. McCaig, A.M. Bahmanpour, D. Ferri, O. Kröcher, Water inhibition of oxymethylene dimethyl ether aynthesis over zeolite H-Beta: a combined kinetic and in situ ATR-IR study, ACS Catal. 10 (2020) 8106–8119, https://doi.org/10.1021/acscatal.0c01805.

[32] Y. Xue, Y. Niu, H. Zheng, X. Cui, Q. Ma, J. Tang, L. Ding, Selective dealumination of ZSM-5 by steaming and its effect on ethanol to propene, J. Fuel Chem. Technol. 49 (2021) 1111–1121, https://doi.org/10.1016/S1872-5813(21)60064-6.
[33] N.R. Meshram, S.G. Hegde, S.B. Kulkarni, Active sites on ZSM-5 zeolites for toluene disproportionation, Zeolites 6 (1986) 434–438, https://doi.org/10.1016/0144-2449(86)90026-6.
[34] M.A. Uguina, J.L. Sotelo, D.P. Serrano, Toluene disproportionation over ZSM-5 zeolite: effects of crystal size, silicon-to-aluminum ratio, activation method and pelletization, Appl. Catal. 76 (1991) 183–198, https://doi.org/10.1016/0166-9834(91)80046-Y.
[35] C. Muhammad, J.A. Onwudili, P.T. Williams, Catalytic pyrolysis of waste plastic from electrical and electronic equipment, J. Anal. Appl. Pyrolysis 113 (2015) 332–339, https://doi.org/10.1016/J.JAAP.2015.02.016.
[36] J.C. Groen, J.C. Jansen, J.A. Moulijn, J. Pérez-Ramírez, Optimal aluminum-assisted mesoporosity development in MFI zeolites by desilication, J. Phys. Chem. B 108 (2004) 13062–13065, https://doi.org/10.1021/jp047194f.
[37] K. Wojtacha-Rychter, N. Howaniec, A. Smoliński, Effect of porous structure of coal on propylene adsorption from gas mixtures, Sci. Rep. 10 (2020) 1–11, https://doi.org/10.1038/s41598-020-67472-x.
[38] W. Widayat, A.N. Annisa, Synthesis and characterization of ZSM-5 catalyst at different temperatures, IOP Conf. Ser. Mater. Sci. Eng. 214 (2017), https://doi.org/10.1088/1757-899X/214/1/012032.
[39] E.S.C. Ferreira, I.V. Voroshylova, V.A. Koverga, C.M. Pereira, M.N.D.S. Cordeiro, New force field model for propylene glycol: Insight to local structure and dynamics, J. Phys. Chem. B 121 (2017) 10906–10921, https://doi.org/10.1021/acs.jpcb.7b08251.
[40] J. Aguado, D.P. Serrano, J.M. Escola, A. Peral, Catalytic cracking of polyethylene over zeolite mordenite with enhanced textural properties, J. Anal. Appl. Pyrolysis 85 (2009) 352–358, https://doi.org/10.1016/j.jaap.2008.10.009.
[41] D.P. Serrano, J.M. Escola, L. Briones, M. Arroyo, Hydroprocessing of the LDPE thermal cracking oil into transportation fuels over Pd supported on hierarchical ZSM-5 catalyst, Fuel 206 (2017) 190–198, https://doi.org/10.1016/j.fuel.2017.06.003.
[42] A. Zachariou, A.P. Hawkins, R.F. Howe, J.M.S. Skakle, N. Barrow, P. Collier, D. W. Nye, R.I. Smith, G.B.G. Stenning, S.F. Parker, D. Lennon, Counting the acid sites in a commercial ZSM-5 zeolite catalyst, ACS Phys. Chem. Au. 3 (2023) 74–83, https://doi.org/10.1021/acsphyschemau.2c00040.
[43] L.E. Sandoval-Díaz, J.A. González-Amaya, C.A. Trujillo, General aspects of zeolite acidity characterization, Microporous Mesoporous Mater. 215 (2015) 229–243, https://doi.org/10.1016/j.micromeso.2015.04.038.
[44] K. Chen, Z. Gan, S. Horstmeier, J.L. White, Distribution of aluminum species in zeolite catalysts: 27Al NMR of framework, partially-coordinated framework, and non-framework moieties, J. Am. Chem. Soc. 143 (2021) 6669–6680, https://doi.org/10.1021/jacs.1c02361.
[45] S.R. Batool, V.L. Sushkevich, J.A. van Bokhoven, Correlating Lewis acid activity to extra-framework aluminum species in zeolite Y introduced by Ion-exchange, J. Catal. 408 (2022) 24–35, https://doi.org/10.1016/j.jcat.2022.02.010.
[46] J.I. Villegas, N. Kumar, T. Heikkilä, V.P. Lehto, T. Salmi, D.Y. Murzin, Isomerization of n-butane to isobutane over Pt-modified Beta and ZSM-5 zeolite catalysts: catalyst deactivation and regeneration, Chem. Eng. J. 120 (2006) 83–89, https://doi.org/10.1016/J.CEJ.2006.03.011.
[47] X. Yu, B. Liu, Y. Zhang, Effect of Si/Al ratio of high-silica HZSM-5 catalysts on the prins condensation of isobutylene and formaldehyde to isoprene, Heliyon 5 (2019), e01640, https://doi.org/10.1016/J.HELIYON.2019.E01640.
[48] R.H. Meinhold, D.M. Bibby, 13C CPMAS n.m.r. study of coke formation on HZSM-5, Zeolites 10 (1990) 121–130, https://doi.org/10.1016/0144-2449(90)90030-U.
[49] J. Kansy, Microcomputer program for analysis of positron annihilation lifetime spectra, Nucl. Instrum. Methods Phys. Res. A 374 (1996) 235–244, https://doi.org/10.1016/0168-9002(96)00075-7.
[50] I. Toshinobu, Okamoto Yasuaki, The isomerization of propylene oxide on zeolite catalysts, Bull. Chem. Soc. Jpn 45 (1972) 3251–3254, https://doi.org/10.1246/bcsj.45.3251.
[51] T. Laino, C. Tuma, P. Moor, E. Martin, S. Stolz, A. Curioni, Mechanisms of propylene glycol and triacetin pyrolysis, J. Phys. Chem. A 116 (2012) 4602–4609, https://doi.org/10.1021/jp300997d.
[52] H.W. Bohnen, B. Cornils, Hydroformylation of alkenes: an industrial view of the status and importance, Adv. Catal. 47 (2002) 1–64, https://doi.org/10.1016/S0360-0564(02)47005-8.
[53] C. Hou, G. Zhao, Y. Ji, Z. Niu, D. Wang, Y. Li, Hydroformylation of alkenes over rhodium supported on the metal-organic framework ZIF-8, Nano Res. 7 (2014) 1364–1369, https://doi.org/10.1007/S12274-014-0501-4.
[54] Y. Wang, L. Yan, C. Li, M. Jiang, Z. Zhao, G. Hou, Y. Ding, Heterogeneous Rh/CPOL-BP&P(OPh)3 catalysts for hydroformylation of 1-butene: the formation and evolution of the active species, J. Catal. 368 (2018) 197–206, https://doi.org/10.1016/J.JCAT.2018.10.012.
[55] J. Zhang, P. Sun, G. Gao, J. Wang, Z. Zhao, Y. Muhammad, F. Li, Enhancing regioselectivity via tuning the microenvironment in heterogeneous hydroformylation of olefins, J. Catal. 387 (2020) 196–206, https://doi.org/10.1016/J.JCAT.2020.03.032.
[56] J. Amsler, B.B. Sarma, G. Agostini, G. Prieto, P.N. Plessow, F. Studt, Prospects of heterogeneous hydroformylation with supported single atom catalysts, J. Am. Chem. Soc. 142 (2020) 5087–5096, https://doi.org/10.1021/jacs.9b12171.
[57] W. Alsalahi, A.M. Trzeciak, Rhodium-catalyzed hydroformylation under green conditions: Aqueous/organic biphasic, “on water”, solventless and Rh nanoparticle based systems, Coord. Chem. Rev. 430 (2021), 213732, https://doi.org/10.1016/J.CCR.2020.213732.
[58] A. Chauvel, G. Lefebvre, Petrochemical Processes: Technical and Economic Characteristics, Editions Technip,, 1989. ⟨https://books.google.com/books?id=ayzjoQEACAAJ⟩.
[59] L. Schweitzer, J. Noblet, I.H. Suffet, The formation, stability, and odor characterization of 2-ethyl-4-methyl-1,3-dioxolane (2-EMD), Water Sci. Technol. 40 (1999) 293–298, https://doi.org/10.1016/S0273-1223(99)00571-5.
[60] A. Fási, I. Pálinkó, I. Kiricsi, Effects of substituents on the ring-opening pathways of oxiranes on ZSM-5 zeolites, React. Kinet. Catal. Lett. 74 (2001) 187–194, https://doi.org/10.1023/A:1017960321702.
[61] A. Lifshitz, C. Tamburu, Isomerization and decomposition of propylene oxide. Studies with a single-pulse shock tube, J. Phys. Chem. 98 (1994) 1161–1170, https://doi.org/10.1021/j100055a020.
[62] M. Sutter, E. da Silva, N. Duguet, Y. Raoul, E. Métay, M. Lemaire, Glycerol ether synthesis: a bench test for green chemistry concepts and technologies, Chem. Rev. 115 (2015) 8609–8651, https://doi.org/10.1021/cr5004002.